ACS EARTH AND SPACE CHEMISTRY

Article

High-Throughput Calibration-Free Laser-Induced Breakdown Spectroscopy

Tarojiro Matsumura,* Tomoko Takahashi, Kenji Nagata, Yasunobu Ando, Akira Yada, Blair Thornton, and Tatsu Kuwatani

Cite This: https://doi.org/10.1021/acsearthspacechem.4c00067

Read Online

ACCESS | Metrics & More | Article Recommendations | Supporting Information

ABSTRACT: Laser-induced breakdown spectroscopy (LIBS) offers a noninvasive, label-free technique for chemical analysis in challenging environments, including for deep-sea mineral resource evaluation and extra-terrestrial geology. We aim to improve the usefulness of LIBS spectral analysis in these applications. We propose an efficient, systematic procedure that uses calibration-free LIBS (CF-LIBS) to quantitatively estimate chemical compositions. This method combines baseline estimation and denoising using sparsity with the spectrum-adapted expectation−conditional maximization algorithm, enabling nonlinear background subtraction and high-throughput peak fitting. In addition, we introduce a Boltzmann plot regression based on Student's *t*-distribution that is robust against outliers. These techniques allow the chemical composition of metal and rock samples to be estimated using the CF-LIBS method, demonstrating its potential for use in comprehensive geological surveys in deep-sea and extra-terrestrial environments.

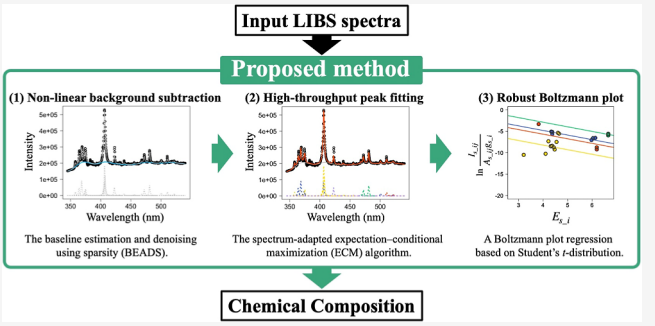

KEYWORDS: *high-throughput spectral data analysis, nonlinear background subtraction, peak fitting, robust Boltzmann plot, CF-LIBS, BEADS, spectrum adapted ECM algorithm*

1. INTRODUCTION

Laser-induced breakdown spectroscopy (LIBS) is a label-free, noncontact elemental analysis technique applicable to a wide range of materials.[1] LIBS requires no sample treatment and the measurements are quick with a rapid response; therefore, it has advantages for in situ measurements in environments that are not easily accessible, including nuclear power plants[2] and on other planets.[3] In particular, LIBS has unique potential for in situ analysis of solid targets submerged in water, where alternative methods are limited. Although signal degradation is often seen in LIBS spectra obtained from targets submerged in water, several techniques have been proposed to improve the signal quality, including double-pulse[4] and long-pulse techniques.[5] Although the double-pulse technique is sensitive to external pressure,[6,7] signal enhancement relative to the conventional single-pulse technique with a pulse duration of several ns is seen up to 30 MPa using the long-pulse technique with a laser pulse duration of ≥150 ns.[8]

One promising target for in situ measurements using the long-pulse LIBS technique is deep-sea minerals, including hydrothermal sulfide deposits and Co−Mn crusts. Although they have received much attention owing to their potential for mining, detailed ore reserve estimates and deep-sea environmental impact assessments are required before their economic potential can be assessed. Deep-sea sediments and rocks are usually sampled then analyzed in a laboratory; however, the inaccessibility of the deep sea limits the number of samples that can be recovered. A deep-sea LIBS analyzer has been developed and successfully deployed in hydrothermal vent fields in the Okinawa Trough, and in situ measurements of metallic elements in hydrothermal deposits have been obtained from multiple locations at water depths of 1000 m.[9]

Quantifying compositions using LIBS spectra in the deep sea has been challenging. Matrix effects due to the physical and chemical properties of the sample affect the quality of the analyses, which limits the applicability of conventional calibration curves. Although calibration curves can be applied to well-resolved peaks when matrix-matched samples are available,[10−12] prior knowledge about the compositions of a target sample is necessary. This is often not the case for natural geological samples,[1] particularly deep-sea minerals.

Practical methods have been investigated to increase the applicability of quantitative analysis, including calibration-free LIBS (CF-LIBS)[13] and multivariate regression[14] (Figure 1). Multivariate regression (e.g., principal component and partial

Received: March 20, 2024
Revised: May 13, 2024
Accepted: May 14, 2024

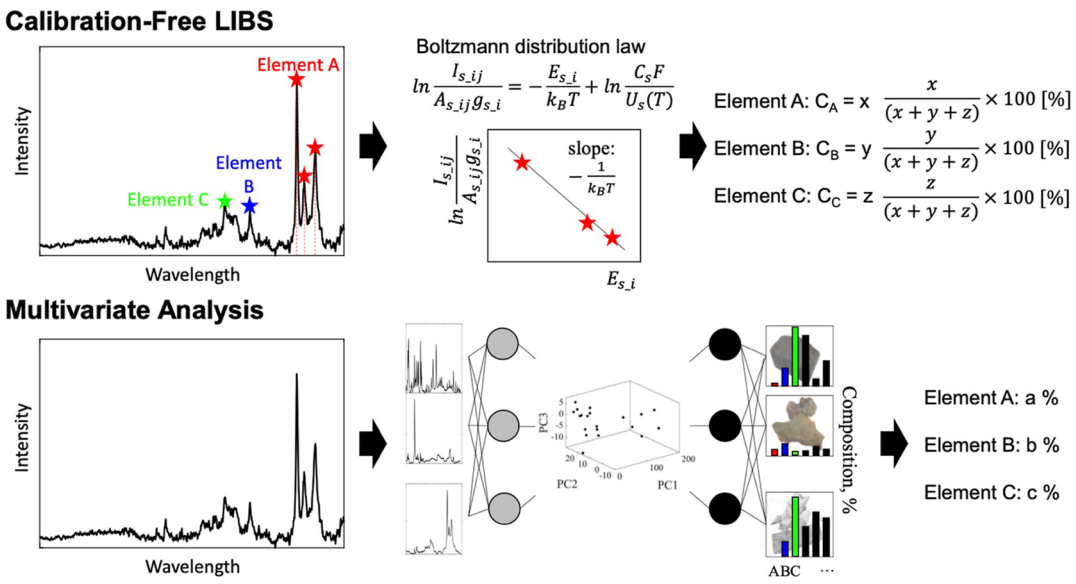

Figure 1. CF-LIBS and multivariate analysis schemes for quantitative LIBS spectral analysis.

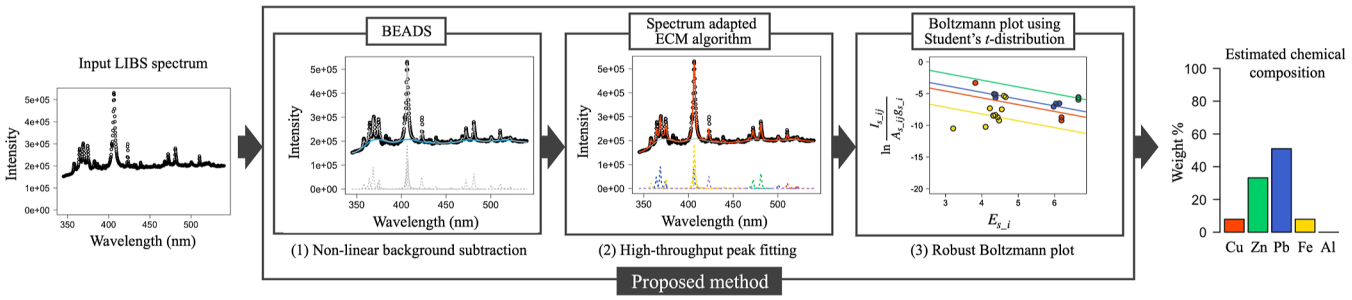

Figure 2. Outline of the proposed method. To obtain the chemical composition from a LIBS spectrum requires three steps: nonlinear background subtraction by BEADS, peak fitting by an ECM algorithm, and robust Boltzmann plot estimation using Student's *t*-distribution.

least-squares regression) takes the matrix effect into account by constructing a regression model using a set of spectra and compositions. These methods have been applied successfully to quantitative analysis of LIBS spectra taken from geological targets with complex matrices on land[15,16] and in situ on Mars.[17−20] Although the large shot-to-shot signal fluctuations from water-submerged samples caused by the instability of underwater plasmas result in poor performance, quantification of major elements in metals and rocks has been successfully conducted using multivariate regression on appropriate spectra and data set pretreatment, including background subtraction or normalization and data set segmentation by chemical parameters.[21,22] Although multivariate regression has the potential for in situ quantitative analysis of deep-sea minerals,[23] a bottleneck is that it still requires reference data sets for samples with similar matrices and in similar environments, even if the matrix effect on quantitative results is mitigated. In contrast, CF-LIBS can be applied without standard samples or preprepared data sets for calibration; therefore, CF-LIBS is a promising technique for quantifying chemical compositions in situ, even for large-scale geological surveys in the deep sea and on other planets where full, preprepared data sets are not always available, as a diverse range of minerals is expected.

Peak fitting of LIBS spectra in water-submerged samples presents challenges during in situ analysis owing to the effect of nonlinear continuum emission, peak broadening, and shot-to-shot fluctuations on peak shape.[24−26] In addition, the complexity of the sample exacerbates the difficulty of peak fitting, as an individual spectrum can contain multiple peaks. Although CF-LIBS offers greater versatility than multivariate analysis for in situ analysis, enhancing the applicability of CF-LIBS requires addressing the challenges associated with peak fitting. These difficulties also hinder accurate chemical analysis, which relies on peak fitting.

To address the difficulties associated with LIBS, we introduce an efficient analysis method based on CF-LIBS. The proposed method combines three techniques: (1) nonlinear background subtraction, (2) high-throughput peak fitting, and (3) robust temperature estimation. The chemical analysis of samples submerged in water requires the component peaks to be obtained and analyzed by peak fitting of LIBS spectra. Using these techniques, our proposed method links peak fitting with compositional analysis. Our proposed method combines baseline estimation and denoising using sparsity (BEADS), the spectrum-adapted expectation−conditional maximization (ECM) algorithm, and maximum likelihood estimation using Student's *t*-distribution. BEADS enable nonlinear background subtraction by separating the series of peaks from the baseline low-pass signal and noise. The spectrum-adapted ECM algorithm conducts high-throughput peak fitting using stable numerical calculations. Maximum likelihood estimation using Student's *t*-distribution provides a Boltzmann plot method for estimating the plasma temperature and chemical compositions that is robust to outliers.

https://doi.org/10.1021/acsearthspacechem.4c00067
ACS Earth Space Chem. XXXX, XXX, XXX−XXX

Combining these methods improves the efficiency of the quantitative analysis of LIBS spectra, with the potential to fully automate and perform the quantification process in situ. Using the proposed method, we determined the chemical compositions of metal and rock samples.

2. METHODS

2.1. Outline of the Proposed Method. LIBS analysis using the proposed method consists of three steps (Figure 2): (1) nonlinear background subtraction, (2) high-throughput peak fitting, and (3) a robust Boltzmann plot. The background is estimated using a majorization−minimization (MM) algorithm, which is an iterative optimization method to find the maximum or minimum of a function.[27] The peaks are then fitted using the ECM algorithm to optimize a pseudo-Voigt mixture model (see the Supporting Information). To estimate the plasma temperature and chemical composition, the slope and intercept of the regression line on a Boltzmann plot are determined using the EM algorithm (see the Supporting Information).

2.2. Calibration-Free LIBS Approach. CF-LIBS was first introduced by Ciucci et al.[28] as a quantitative analytical technique for atomic emission spectroscopy. Element ratios can be determined directly from emission lines by accounting for physical and chemical matrix effects through the application of the Boltzmann distribution.[29] The following assumptions need to be satisfied to use the Boltzmann distribution:[13] local thermal equilibrium, spatial homogeneity, stoichiometric ablation, and the absence of self-absorption (spectral lines used in the calculation are optically thin). The assumption of local thermal equilibrium, spatial homogeneity, and stoichiometric ablations are satisfied for the experimental conditions of this study.[30] To minimize the self-absorption effect, emission lines for which the lower energy level of the transition is on or very close to the ground state were not used for CF-LIBS calculations, following our previous approach using the same experimental setup,[30] as self-absorption could contribute remarkably to those transitions.[31] The CF-LIBS calculation is described in detail in Section "Estimation of Plasma Temperature and Chemical Composition (CFLIBS Calculation)" 2.5.

2.3. Baseline Estimation and Denoising Using Sparsity. Previous studies have reported various approaches for background subtraction from LIBS spectra, including polynomial-based numerical modeling,[32−35] model-free algorithms,[36] and wavelet-based techniques.[37,38] We employ BEADS, a background subtraction technique introduced by ref 27. BEADS is a baseline subtraction method initially proposed for chromatographic data based on signal processing techniques. BEADS has been used in many fields, including biology, biomedical sciences, astronomy, polymer chemistry, and signal monitoring.[39−45] The method is also applicable to any long series of spectral data with combinations of complex nonlinear background and noise with different frequencies and is suitable for processing underwater LIBS spectra. This method splits observed data into the spectrum, background, and Gaussian noise. Given that the background subtracted by BEADS is model-free, there is no need to calculate higher-order polynomials, as is done in conventional LIBS analysis. The calculation is performed using a majorization−minimization approach.[27] The original source code for BEADS is available at the web site.[46]

2.4. Spectrum-Adapted ECM Algorithm. The peak fitting was performed using the spectrum-adapted ECM algorithm.[47−49] This algorithm is a method for efficient and stable peak fitting based on the ECM algorithm,[50] which is a generalized expectation maximization algorithm.[51,52] Iterative expectation and conditional maximization calculations were performed using the intensity of the spectrum as the weight of the corresponding measurement step. The advantages of the spectrum-adapted ECM algorithm include a monotonous increase and convergence of likelihood and sufficient speed for practical peak fitting.[48] Furthermore, the spectrum-adapted ECM algorithm can be applied to various fitting models.[48,49] The fitting procedure is described in the Supporting Information

2.4.1. Fitting Model. We use a pseudo-Voigt mixture model (PVMM) to represent the peak shape. PVMMs are commonly used for LIBS spectral analysis.[53,54] A PVMM is defined as a linear superposition of the m-th normalized pseudo-Voigt distribution $\mathbf{P}_{\mathrm{PV}}(x_n|\mu, \sigma, \eta)$ as follows

$$\mathrm{PVMM}(x_n|\boldsymbol{\mu}, \boldsymbol{\sigma}, \boldsymbol{\eta}, \lambda) = \sum_{m=1}^{M} \lambda_m \mathbf{P}_{\mathrm{PV}}(x_n|\mu_m, \sigma_m, \eta_m) \tag{1}$$

where λ is the proportion of each component ($0 \le \lambda \le 1$ and $\sum_{m=1}^{M} \lambda_m = 1$), and $\mathbf{P}_{\mathrm{PV}}(x_n|\mu, \sigma, \eta)$ can be expressed as

$$\mathbf{P}_{\mathrm{PV}}(x_n|\mu, \sigma, \eta) = \frac{\mathrm{pseudoVoigt}(x_n|\mu, \sigma, \eta)}{\sum_{n=1}^{N} \mathrm{pseudoVoigt}(x_n|\mu, \sigma, \eta)} \tag{2}$$

where

$$\mathrm{pseudoVoigt}(x_n|\mu, \sigma, \eta) = \eta \mathbf{L}(x_n|\mu, \sqrt{2 \ln 2}\,\sigma) + (1 - \eta)\mathbf{N}(x_n|\mu, \sigma) \tag{3}$$

$\mathbf{L}$ and $\mathbf{N}$ are Lorentz and Gauss distributions, respectively, μ is the mean, σ is the standard deviation, and η is the mixing parameter for the Gauss and Lorentz distributions ($0 \le \eta \le 1$). As the distribution has a broad tail and the measurement steps (x_n) are finite, each distribution is truncated over the range of x_n.

We fit the spectral data using a combination of the PVMM and the background model ($\mathbf{B}$)

$$\mathrm{PVMMB}(x_n|\boldsymbol{\mu}, \boldsymbol{\sigma}, \boldsymbol{\eta}, \lambda) = \sum_{m=1}^{M} \lambda_m \mathbf{P}_{\mathrm{PV}}(x_n|\mu_m, \sigma_m, \eta_m) + \lambda_{M+1}\mathbf{B} \tag{4}$$

The first term on the right-hand side of eq 4 corresponds to the peak, and the second term corresponds to the background. In the model fit, the mixture ratio (λ) sums to 1 (i.e., $0 \le \lambda \le 1$, $\sum_{m=1}^{M+1} \lambda_m = 1$).

2.5. Estimation of Plasma Temperature and Chemical Composition (CF-LIBS Calculation). The excitation temperature (hereafter temperature) is estimated using a Boltzmann distribution, as follows

$$\ln \frac{I_{s\_ij}}{A_{s\_ij} g_{s\_i}} = -\frac{E_{s\_i}}{k_B T} + \ln \frac{C_s F}{U_s(T)} \tag{5}$$

where I_{s_ij} is the intensity of the spectral line in arbitrary units (total intensity of a peak), A_{s_ij} is the transition probability (s^{-1}), g_{s_i} is the statistical weight, E_{s_i} is the excitation energy (eV), k_B is the Boltzmann constant (1.38010^{-23} J K^{-1}), T is the temperature (K), C_s is the number density of each emitted species, F is an experimental parameter, and $U_s(T)$ is the

https://doi.org/10.1021/acsearthspacechem.4c00067
ACS Earth Space Chem. XXXX, XXX, XXX−XXX

Table 1. Sample Descriptions

sample name	company/location	Cu (%)	Zn (%)	Pb (%)	Fe (%)	Al (%)	Ba (%)	Ca (%)
31X78355.5	MBH Analytical Ltd.	91.25	6.23	1.64	0.13			
C7701	JCBA[a]	55.01	44.98	0.00	0.01			
HPD1331G05	Hatoma Knoll	6.12	35.1	24.1	6.81	0.30	0.01	0.01
HPD1929R01	Iheya North Knoll	4.53	35.1	7.07	9.68	0.26	0.01	0.04

[a]JCBA: Japan Copper and Brass Association.

partition function. The subscripts i, j, and s refer to the upper, i, and lower, j, energy levels of element s.

We obtained A_{s_ij}, g_{s_i}, and E_{s_i} from the National Institute of Standards and Technology (NIST)[55] and Kurucz atomic spectral line[56] databases. Equation 5 describes a line with an intercept of $\ln \frac{C_s F}{U_s(T)}$ and a slope of $-\frac{1}{k_B T}$ on the $E_{s\_i} - \ln \frac{I_{s\_ij}}{A_{s\_ij} g_{s\_i}}$ plane. As the values of A_{s_ij}, g_{s_i}, and E_{s_i} can be obtained from databases, once I_{s_ij} is determined, the slope and intercept can be obtained using an optimization method. Using the value of the slope, T can also be estimated. The C_s value for all elements with spectral lines identified in the spectrum can be calculated by inputting T into eq 5. The compositional ratios of the detected elements are then obtained by dividing each C_s by the sum of the number densities. It should be noted that the C_s value of singly ionized species should be included in the composition calculation; however, we did not observe any lines from singly ionized species suitable for CF-LIBS. Although it is possible to calculate the density of single ionized species using the Saha equation,[28] there is uncertainty in the calculated electron density due to the Stark broadening effect,[57] particularly in the case of the complex spectra produced by water-submerged rocks. The CF-LIBS calculations are simplified to observed neutral species in this study, in order to compare results between samples. To estimate the intercept and slope, we employed maximum likelihood estimation, which optimizes the model parameters by maximizing a likelihood function. We applied a likelihood function consisting of Student's t-distribution to the data because it is robust against outliers (e.g., Gelman[58] and McElreath[59]). The details of the derivation of the likelihood function are provided in Supporting Information B.

3. LIBS SPECTRA ANALYSIS

3.1. Collection of LIBS Spectra. We used an open LIBS data set published by the University of Tokyo (https://github.com/ocean-perception/chemicam_open_database) and selected data for two metal (31X78355.5 and C7701) and two rock (HPD1331G05 and HPD1929R01) samples. We analyzed 10 spectra (#1−#10) for each sample. The metal samples are commercially available certified alloys, and the rock samples are pelletized samples of rocks collected from deep-sea hydrothermal vent fields in the Okinawa Trough, Japan. The elemental compositions were certified using inductively coupled plasma−atomic emission spectroscopy (ICP−AES) and inductively coupled plasma−mass spectroscopy (ICP−MS) by Activation Laboratories (Actlabs). These are highly accurate quantitative methods and are commonly used to determine mineral compositions, although they cannot be performed in situ, as sample dissolution is required. Table 1 lists detailed sample information. We quantified the elements for which peaks could be detected in both simulations using the known compositions and a Boltzmann distribution (eq 5) for each type of sample: Cu, Zn, and Pb for the metal samples and Cu, Zn, Pb, Fe, Al, Ba, and Ca for the rock samples.

The spectral data were acquired using a LIBS device. The setup is described in our previous work.[26] The plasma was generated on the targets using a custom-built Q-switched Nd:YAG laser with a wavelength of 1064 nm, pulse energy of 5 mJ, and pulse duration of 150 ns. The metal samples were submerged in pure water and the rock samples were submerged in artificial seawater. The laser beam was delivered by an optical fiber and focused onto each target using a custom-made objective lens with 5× magnification connected to the fiber. The light emitted from the plasma passes through a custom-built spectrometer and the spectra are recorded using an intensified charge-coupled device (ICCD). For metal samples, the spectral range was set to 250−570 nm with a resolution of 0.8 nm. For rock samples, the range was set to 320−550 nm with a resolution of 0.25 nm, as higher resolution is required for rock samples because they are expected to have a larger number of peaks. The gate width and delay of the ICCD were set to 500 and 400 ns, respectively, as these values were found to achieve the highest signal-to-noise ratios.

3.2. Initial Parameters. We carried out the peak fitting method for each spectrum. We set the number of peaks, M, to 12 and 34 for the metal and rock samples, respectively. We also added a background component to each fitting model. The initial values of the parameters for the metal and rock samples are listed in Tables 2 and 3, respectively. We fixed μ to the peak positions from the databases.[55,56] As the peak widths in each spectrum are assumed to be equal, a single σ value was estimated for all peak components, whereas individual η and λ values were estimated for each peak component.

Table 2. Initial Peak Fitting Conditions for the Metal Samples

peak	μ	σ	η	λ	element
1	324.8	3	0.9999	1/120	Cu I
2	327.4	3	0.9999	1/120	Cu I
3	510.6	3	0.9999	1/120	Cu I
4	515.3	3	0.9999	1/120	Cu I
5	521.8	3	0.9999	1/120	Cu I
6	334.5	3	0.9999	1/120	Zn I
7	468 3	3	0.9999	1/120	Zn I
8	472.2	3	0.9999	1/120	Zn I
9	481.1	3	0.9999	1/120	Pb I
10	364.0	3	0.9999	1/120	Pb I
11	368.3	3	0.9999	1/120	Pb I
12	405.8	3	0.9999	1/120	Pb I
background	–	–	–	0.9	

For the BEADS, we set the filter order, d, to 1, filter cutoff frequency, f_c, to 0.05, asymmetry ratio, r, to 6, and regularization parameters, λ_0, λ_1, and λ_2, to 0.3, 3, and 2.4, respectively. These hyperparameters were selected heuristi-

https://doi.org/10.1021/acsearthspacechem.4c00067
ACS Earth Space Chem. XXXX, XXX, XXX−XXX

Table 3. Initial Peak Fitting Conditions for the Rock Samples[a]

peak	μ	σ	η	λ	element
1	394.4	3	0.9999	1/340	Al I
2	396.2	3	0.9999	1/340	Al I
3	510.6	3	0.9999	1/340	Cu I
4	515.3	3	0.9999	1/340	Cu I
5	521.8	3	0.9999	1/340	Cu I
6	468.0	3	0.9999	1/340	Zn I
7	472.2	3	0.9999	1/340	Zn I
8	481.1	3	0.9999	1/340	Zn I
9	405.8	3	0.9999	1/340	Pb I
10	357.3	3	0.9999	1/340	Pb I
11	364.0	3	0.9999	1/340	Pb I
12	367.1	3	0.9999	1/340	Pb I
13	368.3	3	0.9999	1/340	Pb I
14	374.0	3	0.9999	1/340	Pb I
15	500.5	3	0.9999	1/340	Pb I
16	520.1	3	0.9999	1/340	Pb I
17	357.0	3	0.9999	1/340	Fe I
18	358.1	3	0.9999	1/340	Fe I
19	372.0	3	0.9999	1/340	Fe I
20	373.5	3	0.9999	1/340	Fe I
21	374.9	3	0.9999	1/340	Fe I
22	382.0	3	0.9999	1/340	Fe I
23	386.0	3	0.9999	1/340	Fe I
24	404.6	3	0.9999	1/340	Fe I
25	406.4	3	0.9999	1/340	Fe I
26	407.2	3	0.9999	1/340	Fe I
27	427.2	3	0.9999	1/340	Fe I
28	430.8	3	0.9999	1/340	Fe I
29	432.6	3	0.9999	1/340	Fe I
30	437.4	3	0.9999	1/340	Fe I
31	438.4	3	0.9999	1/340	Fe I
32	440.5	3	0.9999	1/340	Fe I
33	455.4	3	0.9999	1/340	Ba II
34	422.7	3	0.9999	1/340	Ca I
background				0.9	

[a]Lines marked with an asterisk were not used for the Boltzmann plot estimation, as the lower energy level of the transitions is either the ground state or close to the ground state.

cally. The ends of the spectral data were extended using a logistic function so that both ends decayed smoothly to zero. This technique was introduced as an example of practical data analysis in the Python implementation of BEADS.[60]

The calculation was carried out using R,[61] an open-source programming language and software environment for statistical analysis. On each Boltzmann plot, the initial values of the slope and intercept of the regression line were generated from uniform distributions from −3 to −1 and −50 to 0, respectively. The same values were applied to the slope of the regression line for each spectrum, regardless of the element. The computer carrying out the calculations had an Apple M1Max chip with 10 cores and 32 GB memory.

3.3. Peak Fitting LIBS Spectra. Figure 3 shows the results of fitting spectra 31X78355.5 #1 and C7701 #1. The shape of the model fits the data well. In the model for 31X78355.5 #1, the Cu peak (red dashed line) is dominant, with a minor Zn peak (green dashed line) also being identified. Similarly, in C7701 #1, a major peak for Cu and a minor peak for Zn were identified. Only minor Pb peaks were identified in the models for 31X78355.5 #1 and C7701 #1. These results are consistent with those of previous studies.[30] In addition, the well-fitted curves for the major peaks suggests that the nonlinear background components subtracted by BEADS were appropriate in the region containing the peaks specified by the reference data. However, the background deviates from the data at the edge of the spectrum, near a wavelength of 550 nm. The accuracy of BEADS may be reduced at the edge of the spectrum. However, there are no major peaks at the edge of the spectrum, so the effect on the estimated chemical composition is minimal.

Figure 4 shows the results for HPD1331G05 #1 and HPD1929R01 #1. The model fits the data well. In the model for HPD1331G05 #1, the Fe, Pb, and Zn peaks are prominent, and the Ca peak can also be identified. In addition, the Cu, Al, and Ba peaks are minor. In the model fit for HPD1929R01 #1, the peaks from Fe and Pb are dominant and the peaks from Cu and Zn are minor. In addition, the Al, Ca, and Ba peaks are barely detectable. The Ba content cannot be quantified, as no Ba peak is visible in most spectra. Ca can also not be quantified; reliable results are not expected because of the Ca content of the seawater. Given that well-fitted curves can be obtained for major peaks and the background curve follows the trend of the entire spectrum, BEADS is suitable for the rock data.

3.4. Estimation of the Chemical Composition. Figures 5 and 6 show typical Boltzmann plots for the metal (31X78355.5 #1 and C7701 #1) and rock (HPD1331G05 #1 and HPD1929R01 #1) samples, respectively. The Boltzmann plots for other data are shown in the Supporting Information Although the emission lines listed in Tables 2 and 3 were used for peak fitting (Section 3.3), the following lines were not used for CF-LIBS calculations: 324.8 and 327.4 nm for Cu I from metal samples, and 394.4 nm for Al I, 386.0 nm for Fe I, 455.5 nm for Ba II, and 422.7 nm for Ca I from rock samples. The lower energy levels of the transition that produces these lines are either the ground state or very close to the ground state, and could be affected remarkably by self-absorption. For CF-LIBS calculations for the metal samples, other peaks were also removed, and the following emission lines were used: 510.6, 515.3, and 521.8 nm for Cu I, 481.1 nm for Zn I, and 405.8 nm for Pb I. These lines were selected to compare with the CF-LIBS results from our previous study, whereby these five robust peaks with minimal self-absorption effects were extracted manually from the spectral data used in this study.[30] Although deviation from the Gaussian or Lorentzian peak shapes due to self-absorption should not have a remarkable impact on peak detection, the CF-LIBS calculation is directly affected by self-absorption (Section 2.2). Although the effect of self-absorption on a peak can be evaluated[62] and the peak intensity can be corrected,[63−65] the lines most likely to have been affected by self-absorption were excluded, as our focus is on demonstrating the proposed method for automatic peak detection and fitting, and the calculation of compositions from in situ spectra acquired in a remote environment.

Figure 5 shows that the regression lines for Cu, Zn, and Pb fit the data well. Similarly, Figure 6 shows that the regression lines for Cu, Zn, Pb, Fe, and Al fit the data well. A panel focusing on $\ln \frac{I_{s\_ij}}{A_{s\_ij}g_{s\_i}}$ values of −20 to 0 is also shown. The LIBS spectrum from the rock samples has many peaks, and the intensity of some peaks is low, leading to small values of

https://doi.org/10.1021/acsearthspacechem.4c00067
ACS Earth Space Chem. XXXX, XXX, XXX−XXX

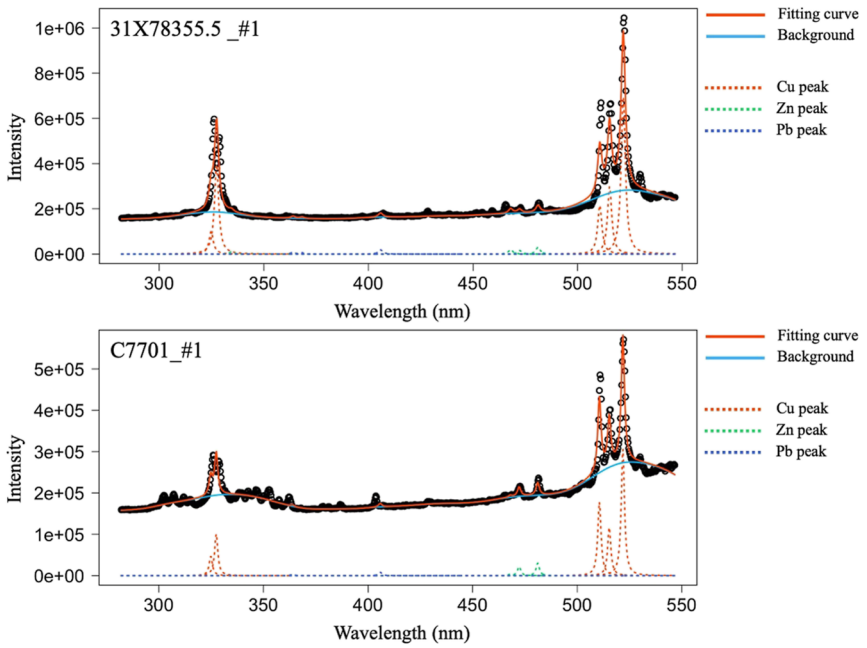

Figure 3. Typical fitting curves for LIBS spectra obtained from metal samples. Top and bottom panels show the model fits for LIBS spectra 31X78355.5_#1 and C7701_#1, respectively. Open circles represent observed data, the model fit and background are shown by solid red and light blue lines, and dotted red, green, and blue dotted lines are the Cu, Zn, and Pb peaks, respectively. Other fitting curves are shown in the Supporting Information (Figures S1 and S2).

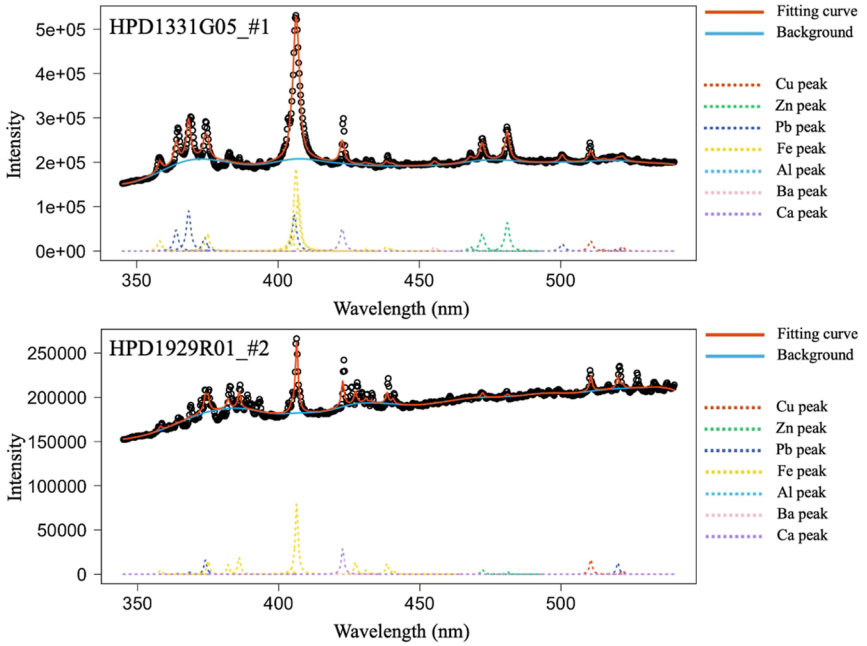

Figure 4. Typical fitting curves for LIBS spectra obtained from rock samples. Top and bottom panels show the model fits for LIBS spectra HPD1331G05_#1 and HPD1929R01_#2, respectively. Open circles represent observed data. Other fitting curves are shown in the Supporting Information (Figures S3 and S4).

$\ln \frac{I_{s\_ij}}{A_{s\_ij}g_{s\_i}}$. The proposed method incorporates a procedure to reduce the influence of this data, so that the regression line will not have an extreme slope. For $\ln \frac{I_{s\_ij}}{A_{s\_ij}g_{s\_i}}$ values of −20 to 0, the regression line passes through a densely populated region of data points, suggesting that the proposed method is robust against outliers, which is a significant advantage. Moreover, the dashed lines represent conventional least-squares regressions.

Our proposed method estimates the plasma temperature, applying the same angular coefficient to all species on a Boltzmann plot. This approach is also required in the established method, where the plasma temperature is estimated using a nonlinear least-squares algorithm.[66] For the metal samples (Figure 5), the regression lines produced by our proposed method are nearly identical to the least-squares regression lines, suggesting little difference between the two approaches in cases with no outliers. In contrast, our proposed

https://doi.org/10.1021/acsearthspacechem.4c00067
ACS Earth Space Chem. XXXX, XXX, XXX−XXX

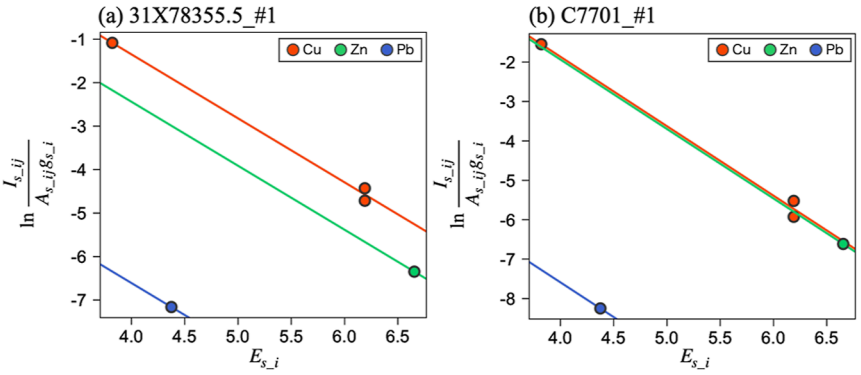

Figure 5. Typical Boltzmann plot for LIBS spectra (a) 31X78,355.5_#1 and (b) C7701_#1. Solid red, green, and blue circles represent Cu, Zn, and Pb, respectively. Red, green, and blue lines are theoretical lines for Cu, Zn, and Pb, respectively. Plots for other spectra are shown in Figures S5 and S6.

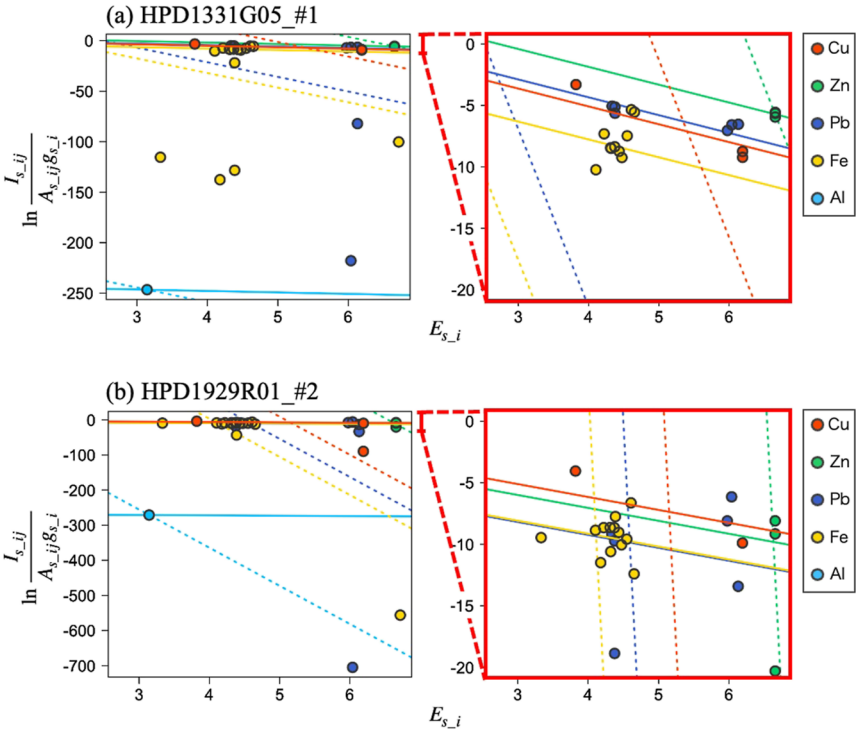

Figure 6. Typical Boltzmann plot for LIBS spectra HPD1331G05_#1 and HPD1929R01_#2 showing (a) the entire range of the data and (b) focusing on $\ln \frac{I_{s\_ij}}{A_{s\_ij} g_{s\_i}}$ values of −20 to 0. Solid red, green, blue, yellow, and light blue circles represent Cu, Zn, Pb, Fe, and Al, respectively, with the corresponding lines representing the theoretical fits for those elements. The dotted lines were obtained using least-squares regressions based on the conventional approach. The slope of the dotted line corresponds to a plasma temperature of <1000 K, which is not realistic for LIBS in water. Plots for other spectra are shown in the Supporting Information (Figures S7−S10).

method showed a noticeable improvement for the rock samples (Figure 5). The regression lines produced using our proposed method intersect the area with many data points, mitigating the effects of outliers, which are often found in the LIBS data for the rock samples in water.

Tables 4−7 list each sample's plasma temperature and chemical composition (wt. %). In the metal samples, the plasma temperatures were estimated to be 5360−9267 K in 31X78355.5 and 6585−8156 K in C7701 (Tables 4 and 5). For the rock samples, the plasma temperatures were estimated to be 7681−11,022 K for HPD1331G05, − 285 K for HPD1929R01 #1, and 5160−12,788 K for HPD1929R01 #2−#10 (Tables 6 and 7). The proposed method produced realistic estimates for the plasma temperatures for all the rock samples, except for HPD1929R01 #1. In contrast, conventional Boltzmann plot estimates of 94−908 K for HPD1331G05 and 86−568 K for HPD1929R01 underestimate the temperature and include impossible values. These results indicate that the proposed method is robust against outliers, allowing for appropriate estimates without complex processing.

The estimated chemical compositions of the metal samples indicate that the majority of sample 31X78355.5 was Cu, and < 3 wt % Pb was detected. In spectra #1−#5 and #10, the Cu content was ∼90 wt % and the Zn content was ∼10 wt %. In spectra #6 and #7, the Cu content was > 95 wt %, with little Zn and Pb being detected. In spectra #8 and #9, the Zn and Pb contents were similar. For sample C7701, the Cu and Zn contents were > 95, and < 2 wt % Pb was detected. The Cu

https://doi.org/10.1021/acsearthspacechem.4c00067
ACS Earth Space Chem. XXXX, XXX, XXX−XXX

Table 4. Plasma Temperatures and Chemical Compositions Estimated Using the Proposed Method for 31X78355.5

31X78355.5	T (K)	Cu (%)	Zn (%)	Pb (%)
#1	7880.20	88.96	9.84	1.20
#2	7935.24	87.97	10.41	1.62
#3	8668.12	86.35	11.39	2.26
#4	8334.68	87.47	10.55	1.98
#5	6902.34	92.78	6.48	0.75
#6	6090.68	96.78	2.64	0.58
#7	5360.76	99.51	0.00	0.49
#8	8876.04	92.24	5.21	2.55
#9	9267.09	93.30	3.62	3.08
#10	7557.56	90.47	8.26	1.28
average	–	91.58 ± 4.00	6.84 ± 3.69	1.58 ± 0.83
ground truth	–	92.06	6.29	1.65

Table 5. Plasma Temperatures and Chemical Compositions Estimated Using the Proposed Method for C7701

C7701	T (K)	Cu (%)	Zn (%)	Pb (%)
#1	6585.85	73.64	25.76	0.59
#2	8099.99	63.56	35.09	1.35
#3	7985.05	63.12	35.69	1.20
#4	8156.32	61.56	37.06	1.38
#5	7007.89	68.18	31.07	0.76
#6	7101.08	66.44	32.76	0.80
#7	7098.48	60.69	38.69	0.62
#8	7900.98	71.35	27.67	0.99
#9	8128.95	58.50	40.23	1.28
#10	7124.42	67.35	31.94	0.71
average	–	65.44 ± 4.57	33.59 ± 4.41	0.97 ± 0.29
ground truth	–	55.01	44.98	0.00

content was > 70 wt % in spectra #1 and #8, and 60 wt % in spectra #7 and #9, lower than the other spectra. In contrast, the Zn content was ∼40 wt %. The estimated minor element (e.g., Zn and Pb) contents in 38X7835.5 are more accurate than those in our previous study, where the peaks were manually extracted.[30] This suggests that the proposed process of peak fitting works reliably for peak extraction, particularly for small peaks, including the 405.8 nm peak for Pb I.

In the rock samples, there were variations in the Cu, Zn, Pb, and Fe contents of HPD1331G05 among the spectra, with Cu contents of 6−21 wt %, Zn, contents of 28−53 wt %, Pb contents of 19−59 wt %, Fe contents of 5−20 wt %, and negligible Al contents in all spectra. Zn is the dominant element in spectra #1 and #4−#7, whereas Pb is the dominant element in spectra #2 and #10. In HPD1929R01, excluding #1, the estimated Cu, Zn, Pb, and Fe contents are 6−66, 0−52, 7−37, and 15−38 wt %, respectively, and the Al content is negligible. There are larger variations in the Cu, Zn, Pb, and Fe contents among the spectra for this sample than for other samples. Cu is the dominant element in spectra #2 and #8, and Zn in spectrum #5. In spectrum #3, the Cu, Zn, Pb, and Fe contents are similar to each other (≈25 ± 5 wt %).

The estimated chemical composition of 31X78355.5 indicates that Cu forms the majority of the sample, the content of Zn is at most ∼10 wt %, and the content of Pb is less than a few wt %, consistent with the accepted chemical composition of the sample. Although there is more variation in the estimated chemical composition of C7701 than that of 31X78355.5, the overall trend (i.e., Cu and Zn comprising the majority of the sample, with Cu being more abundant than Zn and almost no Pb being present) is consistent with the accepted composition. The larger variation in the estimated compositions of C7701 might stem from the sample itself, as 31X78355.5 is a reference standard for analytical use, whereas C7701 is certified for industrial use. The estimated composition of HPD1331G05 shares many features with the accepted composition, e.g., Zn and Pb make up most of the sample, Cu and Fe are minor constituents, and Al is almost absent. The result has a similar or high accuracy compared to our previous study based on a PLS model,[23] and is comparable to other CF-LIBS analysis for geological samples measured on land.[67] However, there are considerable variations in the compositions of HPD1929R01 estimated using our proposed method: spectrum #5 is consistent with the accepted composition, although other results differ from the accepted composition (Table 7). Most of the estimated plasma temperatures are within an empirically realistic range; however, the temperature estimated for HPD1929R01 #1 is unrealistic. This may be due to the trend produced by the dense data points from the Fe peak and may be resolved by applying a proper self-absorption correction. As the proposed method cannot correct for self-absorption, further development of the method is required to ensure more-accurate estimates. In summary, the estimated chemical compositions of samples 31X78355.5, C7701, and HPD1331G05 were mostly consistent with the accepted compositions, whereas that of HPD1929R01 varied from the accepted composition.

Table 6. Plasma Temperatures and Chemical Compositions Estimated Using the Proposed Method for HPD1331G05

HPD1331G05	T (K)	Cu (%)	Zn (%)	Pb (%)	Fe (%)	Al (%)
#1	7976.92	6.47	52.86	35.58	5.08	0.00
#2	7681.46	6.65	27.99	59.18	6.18	0.00
#3	11,022.08	10.10	43.73	26.06	20.12	0.00
#4	9858.58	11.97	50.67	25.13	12.23	0.00
#5	7808.92	10.20	52.73	21.51	15.56	0.00
#6	8829.29	5.98	51.65	36.85	5.53	0.00
#7	8884.25	16.31	50.46	19.08	14.16	0.00
#8	8420.07	21.97	41.93	23.45	12.66	0.00
#9	9203.95	18.17	39.22	25.86	16.74	0.00
#10	8187.78	8.73	39.59	42.99	8.69	0.00
average	–	11.65 ± 5.81	45.08 ± 7.69	31.57 ± 11.68	11.69 ± 4.90	0
ground truth	–	8.45	48.47	33.28	9.40	0.41

https://doi.org/10.1021/acsearthspacechem.4c00067
ACS Earth Space Chem. XXXX, XXX, XXX−XXX

Table 7. Plasma Temperatures and Chemical Compositions Estimated Using the Proposed Method for HPD1929R01[a]

HPD1929R01	T (K)	Cu (%)	Zn (%)	Pb (%)	Fe (%)	Al (%)
#1	−285.88	N/A	N/A	N/A	N/A	N/A
#2	11,037.46	53.13	5.55	6.59	34.73	0.00
#3	10,074.15	20.27	24.36	28.77	26.59	0.00
#4	10,986.96	27.32	15.24	26.08	31.36	0.00
#5	5160.95	5.86	52.38	26.83	14.93	0.00
#6	12,110.75	26.36	12.18	22.82	38.65	0.00
#7	9417.09	31.50	9.57	37.70	21.22	0.00
#8	7812.56	66.18	2.33	12.00	19.49	0.00
#9	8927.28	21.82	22.89	16.86	38.43	0.00
#10	12,788.61	33.11	0.00	31.41	35.48	0.00
average	−	31.73 ± 16.98	16.06 ± 15.09	23.23 ± 9.26	28.99 ± 8.28	0
ground truth	−	8.00	61.97	12.48	17.09	0.46

[a]N/A means "Not applicable".

4. DISCUSSION

4.1. Implications of the Proposed Method for CF-LIBS. The proposed method successfully links peak fitting with compositional analysis based on CF-LIBS by integrating nonlinear background subtraction, efficient peak fitting, and robust temperature estimation. The novel aspects of our method are the use of (1) BEADS for nonlinear background subtraction, (2) the spectrum-adapted ECM algorithm for efficient peak fitting, and (3) maximum likelihood estimation using Student's t-distribution for robust temperature estimation. Each technique enhances the overall efficiency and robustness of LIBS spectra analysis.

We have demonstrated the practical application of the proposed method for determining the chemical composition of metal and rock samples submerged in water. The curves fit the measured spectra well, accurately subtracting even nonlinear background. Robust Boltzmann plot regressions using the peak parameters produced estimated chemical compositions that are consistent with the accepted compositions. The estimated chemical compositions of 31X78355.5 are consistent with the accepted composition. Although there was some variation in the estimated chemical compositions of C7701 and HPD1331G05, the compositional trends were consistent with the accepted compositions (Tables 4−6). These results suggest that the proposed method offers sufficient accuracy for practical LIBS spectral analysis. However, the estimated chemical composition of HPD1929R01 exhibited considerable variation and deviated from the accepted composition (Table 7), particularly spectra #2, #8, and #10. These spectra have extremely strong emission lines from some elements, which are assumed to be reflected in the calculated compositions. As shown by Takahashi et al.,[23] the rock samples used in this study are locally homogeneous. Although the variation in the compositions estimated in this study was larger than seen in analyses of the surface of the sample using X-ray fluorescence,[23] it may be that the spectra were recorded at a point where mineral grains were concentrated, and the variation is within a reasonable range. The proposed method should be applied to a larger data set with a broader range of sample types for further evaluation of its accuracy, which we will study in future.

The proposed method tends to overestimate the background at the edges of the spectrum. Representative examples can be seen at the edge (500−550 nm) of the spectra from the metal samples (31X78355.5 and C7701). We used the peak parameters from these spectra to obtain chemical compositions that are consistent with the accepted compositions. Therefore, we conclude that the effect of this overestimate is small in practice.

As the slope of the regression line is the same for each element, even for elements with few data or limited variation, the analysis can be performed using the data for all elements. Thus, it is unlikely that the plasma temperatures estimated in this study contain considerable errors. However, it is possible that limited data or variation may produce errors or unrealistic results. The proposed method uses maximum likelihood estimation, and it is difficult to evaluate the errors or provide constraints on the model to avoid unrealistic results. To address this problem, the proposed method can be extended with Bayesian inference, which can provide probabilistic constraints on model parameters and evaluate the error distribution. However, there are challenges in extending the proposed method, including restructuring the statistical model for Bayesian inference and implementing a method for in situ measurements with low computational cost. Further work is required to address these issues.

The advantage of the proposed method lies in the increased efficiency of the LIBS spectral analyses it provides. Using BEADS and the spectrum-adapted ECM algorithm enables complex background subtraction and peak fitting, which are traditionally dependent on trial and error, to be completed using a single calculation. In addition, the proposed robust Boltzmann plot method simplifies estimation of chemical compositions. In the conventional Boltzmann plot approach, linear regression is performed using a least-squares method. However, this conventional approach is susceptible to outliers, which could result in significant variations in the estimate owing to a few small peaks. Outliers are particularly common when analyzing sediments and rocks in water using LIBS because their chemical compositions are highly heterogeneous. The proposed method mitigates the effect of outliers systematically, preventing unreasonable plasma temperature estimates. On a conventional Boltzmann plot, outliers are removed to improve the accuracy of the results. However, manually selecting data for removal could introduce bias, which can impede the reproducibility of the analysis. Furthermore, difficult-to-achieve data collection is required to obtain ideal results free from outliers, possibly leading to higher costs. In contrast, our method allows for chemical analysis that uses all the measured data. By addressing these issues, our approach connects spectral measurement to data analysis, contributing to the broader applicability of LIBS. Our

https://doi.org/10.1021/acsearthspacechem.4c00067
ACS Earth Space Chem. XXXX, XXX, XXX−XXX

proposed method is an effective and systematic technique for a wide range of spectrometers and corresponding compositional analyses.

The proposed method focuses on high-throughput analysis of in situ LIBS for submerged samples. In such analyses, it is difficult to obtain high-resolution spectra due to limitations imposed by the power supply and the portability of the equipment. Therefore, peak fitting is time-consuming and practically impossible to complete in situ. There is a need for in situ analysis of LIBS spectra collected from broad areas, especially high-throughput techniques. The proposed method accommodates these needs by improving the efficiency of the peak fitting, and direct estimates of the chemical composition enhance the efficiency of in situ LIBS analysis.

We focused on LIBS analysis of samples submerged in water, but the proposed method can be applied to other spectroscopic techniques. The advantage of our proposed method is that it leads to rapid in situ analysis and dynamic exploration that is robust to outliers. Identifying and removing outliers and anomalous data in advance is complex, and manual selection requires significant time and resources; our method eliminates the need for such preprocessing, thus improving efficiency. The quality of samples in in situ analysis varies, and the samples may include outliers. A robust analysis method can mitigate the effects of outliers and remain accurate.

4.2. Limitations of the Proposed Method. Our proposed method has limitations that warrant refinement and further development. In general, BEADS requires hyperparameter tuning, which affects the peak fitting and computational cost. There are similar limitations in the robust Boltzmann plot technique. For hyperparameter tuning, systematic search methods, including grid search and Bayesian optimization, can be used. This can significantly reduce trial-and-error, thus saving time and cost. In the future, these search techniques will be incorporated into the proposed method. Furthermore, peak fitting depends on reference data. Although the construction of suitable reference data is the out of the scope of the proposed method, it is an essential issue for high-quality spectral analysis. In practice, the proposed method requires appropriate reference data to be prepared based on expert knowledge of the LIBS spectra and previous research in related fields. Although the proposed method improves analysis efficiency, it has yet to be automated. A fully automated quantification process for mineral compositions on the seafloor will enable long-duration operations that are not limited by the sampling capability of submersibles, thus significantly increasing survey efficiency. In addition, in situ quantitative results can provide real-time feedback to allow surveys to focus efficiently on areas of interest. Further research is necessary to increase both the accuracy and convergence speed. Techniques such as maximum posterior probability estimation and Bayesian estimation could be used to further refine our method by incorporating prior knowledge into the model.[68] Using probabilistic models, these techniques can address constraints, including the feasible range of each parameter. However, these methods will likely complicate the calculation and increase computational costs. Addressing these computational challenges is crucial, and work is ongoing to overcome this and further improve our proposed method.

Another limitation is that we do not fully correct for self-absorption, and this could affect the result. Addressing self-absorption is critical for CF-LIBS. In particular, self-absorption lines tend to have lower intensities than theory suggests,[69] thereby affecting the accuracy of the temperature estimates.

It is difficult to handle self-absorption in analyses of samples submerged in water. Rock data (HPD1331G05 and HPD1929R01) have complex spectra with many peaks, unknown chemical compositions, and considerable noise; therefore, it is difficult to correct for self-absorption. It is also difficult to analyze these spectral data using conventional least-squares approaches. In contrast, the proposed method enables the analysis of these spectra, which is a notable contribution in the on-site CF-LIBS. Some peaks in the rock data are orders of magnitude smaller than the major peaks and are therefore outliers. When estimating the chemical composition from a single spectrum, reducing the influence of outliers can improve the quality of the analysis. The proposed method reduces the influence of outliers using Student's *t*-distribution, and we obtained reasonable results. One of the expected causes of outliers is the self-absorption effect. Although the relationship between outliers and self-absorption is unclear, an extension of the proposed method to include a self-absorption correction would lead to more accurate and reliable estimates of the chemical compositions. In addition, although only neutral species are considered in this study, future studies will include contribution of ionized species in CF-LIBS calculation. The core of the proposed method is the ECM algorithm. As the ECM algorithm has stable computational behavior and flexible scalability, the proposed method can potentially be extended to include self-absorption corrections using efficient parameter optimization.

5. CONCLUSIONS

LIBS is a powerful technique for chemical analysis in challenging environments, including underwater settings. This study introduced an efficient approach for analyzing LIBS spectra, which increases the efficiency of LIBS spectral analyses by using BEADS and the spectrum-adapted ECM algorithm. This approach allows complex analyses, which are typically reliant on trial and error, to be performed using a series of calculations. A Robust Boltzmann plot method also simplifies the estimation of chemical compositions. However, our method does have limitations, including sensitivity to hyperparameters and dependence on initial values, which need to be addressed before it can be fully automated. Incorporating prior knowledge could further refine the method, improving the accuracy, but this may also increase computational costs. We are working to overcome these issues and further refine the technique.

■ ASSOCIATED CONTENT

Supporting Information

The Supporting Information is available free of charge at https://pubs.acs.org/doi/10.1021/acsearthspacechem.4c00067.

Description of the calculation procedure of the spectrum-adapted ECM algorithm for peak fitting, theoretical outline of the Boltzmann plot using Student's *t*-distribution, plots showing analysis result for each LIBS spectrum, fitting curves, and Boltzmann plots (PDF)

https://doi.org/10.1021/acsearthspacechem.4c00067
ACS Earth Space Chem. XXXX, XXX, XXX−XXX

AUTHOR INFORMATION

Corresponding Author

Tarojiro Matsumura − *Research Center for Computational Design of Advanced Functional Materials (CD-FMat), National Institute of Advanced Industrial Science and Technology (AIST), Tsukuba 305-8568 Ibaraki, Japan;* orcid.org/0000-0001-9950-509X; Email: matsumura-tarojiro@aist.go.jp

Authors

Tomoko Takahashi − *Research Institute for Global Change (RIGC), Japan Agency for Marine-Earth Science and Technology (JAMSTEC), Yokosuka 237-0061 Kanagawa, Japan;* orcid.org/0000-0002-2916-7205

Kenji Nagata − *Center for Basic Research on Materials, National Institute for Materials Science (NIMS), Tsukuba 305-0044 Ibaraki, Japan*

Yasunobu Ando − *Research Center for Computational Design of Advanced Functional Materials (CD-FMat), National Institute of Advanced Industrial Science and Technology (AIST), Tsukuba 305-8568 Ibaraki, Japan;* orcid.org/0000-0003-3702-034X

Akira Yada − *Interdisciplinary Research Center for Catalytic Chemistry, National Institute of Advanced Industrial Science and Technology (AIST), Tsukuba 305-8566 Ibaraki, Japan*

Blair Thornton − *Institute of Industrial Science, The University of Tokyo, Meguro 153-8505 Tokyo, Japan*

Tatsu Kuwatani − *Research Institute for Marine Geodynamics (IMG), Japan Agency for Marine-Earth Science and Technology (JAMSTEC), Yokosuka 237-0061 Kanagawa, Japan*

Complete contact information is available at: https://pubs.acs.org/10.1021/acsearthspacechem.4c00067

Notes

The authors declare no competing financial interest.

ACKNOWLEDGMENTS

This work was supported by KAKENHI (20H02747 and 21H01557), JST CREST (JPMJCR1761), Grant-in-Aid for Challenging Research (Exploratory) (22K18742), Sumitomo Foundation grants for Environmental Research Projects (203122) and Basic Science Research Projects (190769), and the Cooperative Research Program of the Earthquake Research Institute, University of Tokyo (2021-B01).

REFERENCES

(1) Hahn, D. W.; Omenetto, N. Laser-induced breakdown spectroscopy (LIBS), part II: review of instrumental and methodological approaches to material analysis and applications to different fields. *Appl. Spectrosc.* **2012**, *66*, 347−419.

(2) Whitehouse, A.; Young, J.; Botheroyd, I.; Lawson, S.; Evans, C.; Wright, J. Remote material analysis of nuclear power station steam generator tubes by laser-induced breakdown spectroscopy. *Spectrochimica Acta Part B: Atomic Spectrosc.* **2001**, *56*, 821−830.

(3) Wiens, R. C.; Maurice, S.; Barraclough, B.; Saccoccio, M.; Barkley, W. C.; Bell, J. F.; Bender, S.; Bernardin, J.; Blaney, D.; Blank, J.; et al. The ChemCam Instrument Suite on the Mars Science Laboratory (MSL) Rover: Body Unit and Combined System Tests. *Space Sci. Rev.* **2012**, *170*, 167−227.

(4) Nyga, R.; Neu, W. Double-pulse technique for optical emission spectroscopy of ablation plasmas of samples in liquids. *Optical Lett.* **1993**, *18*, 747−749.

(5) Sakka, T.; Oguchi, H.; Masai, S.; Hirata, K.; Ogata, Y. H.; Saeki, M.; Ohba, H. Use of a long-duration ns pulse for efficient emission of spectral lines from the laser ablation plume in water. *Appl. Phys. Lett.* **2006**, *88*, 061120.

(6) De Giacomo, A.; De Bonis, A.; Dell'Aglio, M.; De Pascale, O.; Gaudiuso, R.; Orlando, S.; Santagata, A.; Senesi, G. S.; Taccogna, F.; Teghil, R. Laser Ablation of Graphite in Water in a Range of Pressure from 1 to 146 atm Using Single and Double Pulse Techniques for the Production of Carbon Nanostructures. *J. Phys. Chem. C* **2011**, *115*, 5123−5130.

(7) Takahashi, T.; Thornton, B.; Ura, T. Investigation of Influence of Hydrostatic Pressure on Double-Pulse Laser-Induced Breakdown Spectroscopy for Detection of Cu and Zn in Submerged Solids. *Appl. Phys. Express* **2013**, *6*, 042403.

(8) Thornton, B.; Sakka, T.; Takahashi, T.; Tamura, A.; Masamura, T.; Matsumoto, A. Spectroscopic Measurements of Solids Immersed in Water at High Pressure Using a Long-Duration Nanosecond Laser Pulse. *Appl. Phys. Exp.* **2013**, *6*, 082401.

(9) Thornton, B.; Takahashi, T.; Sato, T.; Sakka, T.; Tamura, A.; Matsumoto, A.; Nozaki, T.; Ohki, T.; Ohki, K. Development of a deep-sea laser-induced breakdown spectrometer for in situ multi-element chemical analysis. *Deep-Sea Res. Part I* **2015**, *95*, 20−36.

(10) Eppler, A. S.; Cremers, D. A.; Hickmott, D. D.; Ferris, M. J.; Koskelo, A. C. Matrix effects in the detection of Pb and Ba in soils using laser-induced breakdown spectroscopy. *Appl. Spectrosc.* **1996**, *50*, 1175−1181.

(11) Sun, Q.; Tran, M.; Smith, B. W.; Winefordner, J. D. Zinc analysis in human skin by laser induced-breakdown spectroscopy. *Talanta* **2000**, *52*, 293−300.

(12) Capitelli, F.; Colao, F.; Provenzano, M.; Fantoni, R.; Brunetti, G.; Senesi, N. Determination of heavy metals in soils by laser induced breakdown spectroscopy. *Geoderma* **2002**, *106*, 45−62.

(13) Tognoni, E.; Cristoforetti, G.; Legnaioli, S.; Palleschi, V. Calibration-free laser-induced breakdown spectroscopy: state of the art. *Spectrochim. Acta Part B* **2010**, *65* (1), 1−14.

(14) Pořízka, P.; Klus, J.; Képeš, E.; Prochazka, D.; Hahn, D. W.; Kaiser, J. On the utilization of principal component analysis in laser-induced breakdown spectroscopy data analysis, a review. *Spectrochim. Acta Part B* **2018**, *148*, 65−82.

(15) Wisbrun, R.; Schechter, I.; Niessner, R.; Schroeder, H.; Kompa, K. L. Detector for trace elemental analysis of solid environmental samples by laser plasma spectroscopy. *Anal. Chem.* **1994**, *66*, 2964−2975.

(16) Essington, M. E.; Melnichenko, G. V.; Stewart, M. A.; Hull, R. A. Soil metals analysis using laser-induced breakdown spectroscopy (LIBS). *Soil Sci. Soc. Am. J.* **2009**, *73*, 1469−1478.

(17) Wiens, R.; Maurice, S.; Lasue, J.; Forni, O.; Anderson, R.; Clegg, S.; Bender, S.; Blaney, D.; Barraclough, B.; Cousin, A.; et al. Pre-flight calibration and initial data processing for the ChemCam laser-induced breakdown spectroscopy instrument on the Mars Science Laboratory rover. *Spectrochim. Acta Part B At. Spectrosc.* **2013**, *82*, 1−27.

(18) Clegg, S. M.; Wiens, R.; Misra, A. K.; Sharma, S. K.; Lambert, J.; Bender, S.; Newell, R.; Nowak-Lovato, K.; Smrekar, S.; Dyar, M. D.; Maurice, S. Planetary geochemical investigations using Raman and laser-induced breakdown spectroscopy. *Appl. Spectrosc.* **2014**, *68*, 925−936.

(19) Anderson, R.; Bridges, J.; Williams, A.; Edgar, L.; Ollila, A.; Williams, J.; Nachon, M.; Mangold, N.; Fisk, M.; Schieber, J.; et al. ChemCam results from the Shaler outcrop in Gale crater, Mars. *Icarus* **2015**, *249*, 2−21.

(20) Maurice, S.; Clegg, S. M.; Wiens, R. C.; Gasnault, O.; Rapin, W.; Forni, O.; Cousin, A.; Sautter, V.; Mangold, N.; Le Deit, L.; et al. ChemCam activities and discoveries during the nominal mission of the Mars Science Laboratory in Gale crater, Mars. *J. Anal. At. Spectrom.* **2016**, *31*, 863−889.

(21) Takahashi, T.; Thornton, B.; Sato, T.; Ohki, T.; Ohki, K.; Sakka, T. Temperature based segmentation for spectral data of laser-

induced plasmas for quantitative compositional analysis of brass alloys submerged in water. *Spectrochim. Acta Part B* **2016**, *124*, 87−93.
(22) Takahashi, T.; Thornton, B.; Sato, T.; Ohki, T.; Ohki, K.; Sakka, T. Partial least squares regression calculation for quantitative analysis of metals submerged in water measured using laser-induced breakdown spectroscopy. *Appl. Opt.* **2018**, *57*, 5872−5883.
(23) Takahashi, T.; Yoshino, S.; Takaya, Y.; Nozaki, T.; Ohki, K.; Ohki, T.; Sakka, T.; Thornton, B. Quantitative in situ mapping of elements in deep-sea hydrothermal vents using laser-induced breakdown spectroscopy and multivariate analysis. *Deep Sea Res. Part I* **2020**, *158*, 103232.
(24) Sakka, T.; Iwanaga, S.; Ogata, Y. H.; Matsunawa, A.; Takemoto, T. Laser ablation at solid−liquid interfaces: An approach from optical emission spectra. *J. Chem. Phys.* **2000**, *112*, 8645−8653.
(25) Ushida, H.; Takada, N.; Sasaki, K. Diagnostics of liquid-phase laser ablation plasmas by spectroscopic methods. *J. Phy. Conf. Ser.* **2007**, *59*, 563−566.
(26) Yoshino, S.; Thornton, B.; Takahashi, T.; Takaya, Y.; Nozaki, T. Signal preprocessing of deep-sea laser-induced plasma spectra for identi fi cation of pelletized hydrothermal deposits using Arti fi cial Neural Networks. *Spectrochim. Acta Part B* **2018**, *145*, 1−7.
(27) Ning, X.; Selesnick, I. W.; Duval, L. Chromatogram baseline estimation and denoising using sparsity (BEADS). *Chemom. Intell. Lab. Syst.* **2014**, *139*, 156−167.
(28) Ciucci, A.; Corsi, M.; Palleschi, V.; Rastelli, S.; Salvetti, A.; Tognoni, E. New procedure for quantitative elemental analysis by laser-induced plasma spectroscopy. *Appl. Spectrosc.* **1999**, *53*, 960−964.
(29) Takahashi, T.; Thornton, B. Quantitative methods for compensation of matrix effects and self-absorption in Laser Induced Breakdown Spectroscopy signals of solids. *Spectrochim. Acta Part B* **2017**, *138*, 31−42.
(30) Takahashi, T.; Thornton, B.; Ohki, K.; Sakka, T. Calibration-free analysis of immersed brass alloys using long-ns-duration pulse laser-induced breakdown spectroscopy with and without correction for nonstoichiometric ablation. *Spectrochim. Acta Part B* **2015**, *111*, 8−14.
(31) Cremers, D. A.; Radziemski, L. J. *Handbook of Laser-Induced Breakdown Spectroscopy*; John Wiley & Sons, 2006; .
(32) Gornushkin, I.; Eagan, P.; Novikov, A.; Smith, B.; Winefordner, J. Automatic correction of continuum background in laser-induced breakdown and Raman spectrometry. *Appl. Spectrosc.* **2003**, *57*, 197−207.
(33) Sun, L.; Yu, H. Automatic estimation of varying continuum background emission in laser-induced breakdown spectroscopy. *Spectrochim. Acta Part B* **2009**, *64*, 278−287.
(34) Motto-Ros, V.; Moncayo, S.; Trichard, F.; Pelascini, F. Investigation of signal extraction in the frame of laser induced breakdown spectroscopy imaging. *Spectrochim. Acta Part B* **2019**, *155*, 127−133.
(35) Tan, B.; Huang, M.; Zhu, Q.; Guo, Y.; Qin, J. Detection and correction of laser induced breakdown spectroscopy spectral background based on spline interpolation method. *Spectrochim. Acta Part B* **2017**, *138*, 64−71.
(36) Yaroshchyk, P.; Eberhardt, J. E. Automatic correction of continuum background in Laser-induced Breakdown Spectroscopy using a model-free algorithm. *Spectrochim. Acta Part B* **2014**, *99*, 138−149.
(37) Cousin, A.; Forni, O.; Maurice, S.; Gasnault, O.; Fabre, C.; Sautter, V.; Wiens, R.; Mazoyer, J. Laser induced breakdown spectroscopy library for the Martian environment. *Spectrochim. Acta Part B* **2011**, *66*, 805−814.
(38) Lin, Z.; Zhang, N.; Xu, Z.; Liao, J.; Yuan, H.; Chenshen, E.; Liu, J.; Li, J.; Zhao, N.; Zhang, Q. Modified iterative wavelets for background removal in laser-induced breakdown spectroscopy based on fiber laser ablation. *J. Anal. At. Spectrom.* **2022**, *37*, 2082−2088.
(39) Schulze, H. G.; Turner, R. F. Development and integration of block operations for data invariant automation of digital preprocessing and analysis of biological and biomedical Raman spectra. *Appl. Spectrosc.* **2015**, *69*, 643−664.
(40) Bacher, R.; Chatelain, F.; Michel, O. An adaptive robust regression method: Application to galaxy spectrum baseline estimation. *2016 IEEE International Conference on Acoustics, Speech and Signal Processing (ICASSP)*, 2016; pp 4423−4427..
(41) Qaraqe, M.; Ismail, M.; Serpedin, E.; Zulfi, H. Epileptic seizure onset detection based on EEG and ECG data fusion. *Epilepsy Behav.* **2016**, *58*, 48−60.
(42) Erny, G. L.; Acunha, T.; Simó, C.; Cifuentes, A.; Alves, A. Background correction in separation techniques hyphenated to high-resolution mass spectrometry−Thorough correction with mass spectrometry scans recorded as profile spectra. *J. Chromatogr. A* **2017**, *1492*, 98−105.
(43) Mostafavi, S.; Troxler, J.; Cox, R. W. An unsupervised approach for disaggregating major loads in small commercial buildings *2017 IEEE Energy Conversion Congress and Exposition (ECCE)*, 2017; pp 1575−1581..
(44) Rothensteiner, M.; Jenni, J.; Emerich, H.; Bonk, A.; Vogt, U. F.; van Bokhoven, J. A. In situ flow cell for combined X-ray absorption spectroscopy, X-ray diffraction, and mass spectrometry at high photon energies under solar thermochemical looping conditions. *Rev. Sci. Instrum.* **2017**, *88*, 083116.
(45) Martin, B.; Puentes, J.; Wruck, L.; Osswald, T. A. Degree of cure of epoxy/acrylic photopolymers: Characterization with raman spectroscopy and a modified phenomenological model. *Polym. Eng. Sci.* **2018**, *58*, 228−237.
(46) Duval, L. BEADS: Baseline Estimation And Denoising with Sparsity [online]. http://www.laurent-duval.eu/siva-beads-baseline-background-removal-filtering-sparsity.html (accessed May 10, 2024).
(47) Matsumura, T.; Nagamura, N.; Akaho, S.; Nagata, K.; Ando, Y. Spectrum adapted expectation−maximization algorithm for high−throughput peak shift analysis. *Sci. Technol. Adv. Mater.* **2019**, *20*, 733−745.
(48) Matsumura, T.; Nagamura, N.; Akaho, S.; Nagata, K.; Ando, Y. Spectrum adapted expectation−conditional maximization algorithm for extending high−throughput peak separation method in XPS analysis. *Sci. Technol. Adv. Mater. Methods* **2021**, *1* (1), 45−55.
(49) Matsumura, T.; Nagamura, N.; Akaho, S.; Nagata, K.; Ando, Y. High-throughput XPS spectrum modeling with autonomous background subtraction for 3 d 5/2 peak mapping of SnS. *Sci. Technol. Adv. Mater. Methods* **2023**, *3*, 2159753.
(50) Meng, X.-L.; Rubin, D. B. Maximum likelihood estimation via the ECM algorithm: A general framework. *Biometrika* **1993**, *80*, 267−278.
(51) Dempster, A. P.; Laird, N. M.; Rubin, D. B. Maximum likelihood from incomplete data via the EM algorithm. *J. R. Stat. Soc. Ser. B* **1977**, *39*, 1−22.
(52) McLachlan, G. J.; Krishnan, T. *The EM Algorithm and Extensions*, 2nd ed.; Wiley: New York, 2008.
(53) Aguilera, J. A.; Aragón, C.; Cristoforetti, G.; Tognoni, E. Application of calibration-free laser-induced breakdown spectroscopy to radially resolved spectra from a copper-based alloy laser-induced plasma. *Spectrochim. Acta Part B* **2009**, *64*, 685−689.
(54) Fantoni, R.; Almaviva, S.; Caneve, L.; Colao, F.; Maddaluno, G.; Gasior, P.; Kubkowska, M. Hydrogen isotope detection in metal matrix using double-pulse laser-induced breakdown-spectroscopy. *Spectrochim. Acta Part B* **2017**, *129*, 8−13.
(55) Kramida, A.; Ralchenko, Y.; Reader, J.; NIST ASD Team, *Nist Atomic Spectra Database*, 2023 (version 5.0) [online]. http://physics.nist.gov/asd (accessed Mar 15, 2014).
(56) Smith, P.; Heise, C.; Esmond, J.; Kurucz, R. Kurucz Atomic Line Database [online]. http://www.cfa.harvard.edu/amdata/ampdata/kurucz23/sekur.html (accessed Mar 15, 2014).
(57) Hahn, D. W.; Omenetto, N. Laser-induced breakdown spectroscopy (LIBS), part I: review of basic diagnostics and plasma−particle interactions: still-challenging issues within the analytical plasma community. *Appl. Spectrosc.* **2010**, *64*, 335A−336A.

https://doi.org/10.1021/acsearthspacechem.4c00067
ACS Earth Space Chem. XXXX, XXX, XXX−XXX

(58) Gelman, A.; Hill, J.; Vehtari, A. *Regression and Other Stories*; Cambridge University Press, 2020.
(59) McElreath, R. *Statistical Rethinking: A Bayesian Course with Examples in R and Stan*; CRC Press, 2020.
(60) Skotaro, Pybeads [online]. https://github.com/skotaro/pybeads (accessed May 10, 2024).
(61) CRAN, The Comprehensive R Archive Network [online]. https://cran.r-project.org (accessed May 10, 2024).
(62) Bredice, F.; Borges, F.; Sobral, H.; Villagran-Muniz, M.; Di Rocco, H. O.; Cristoforetti, G.; Legnaioli, S.; Palleschi, V.; Pardini, L.; Salvetti, A.; et al. Evaluation of self-absorption of manganese emission lines in Laser Induced Breakdown Spectroscopy measurements. *Spectrochim. Acta Part B* **2006**, *61*, 1294−1303.
(63) Bredice, F. O.; Rocco, H. O. D.; Sobral, H. M.; Villagrán-Muniz, M.; Palleschi, V. A new method for determination of self-absorption coefficients of emission lines in laser-induced breakdown spectroscopy experiments. *Appl. Spectrosc.* **2010**, *64*, 320−323.
(64) Bulajic, D.; Corsi, M.; Cristoforetti, G.; Legnaioli, S.; Palleschi, V.; Salvetti, A.; Tognoni, E. A procedure for correcting self-absorption in calibration free-laser induced breakdown spectroscopy. *Spectrochim. Acta Part B* **2002**, *57*, 339−353.
(65) Amamou, H.; Bois, A.; Ferhat, B.; Redon, R.; Rossetto, B.; Matheron, P. Correction of self-absorption spectral line and ratios of transition probabilities for homogeneous and LTE plasma. *J. Quant. Spectrosc. Radiat. Transfer* **2002**, *75*, 747−763.
(66) Dennis, J. E.; Gay, D. M.; Walsh, R. E. An adaptive nonlinear least-squares algorithm. *ACM Trans. Math. Software* **1981**, *7* (3), 348−368.
(67) Qiao, S.; Ding, Y.; Tian, D.; Yao, L.; Yang, G. A review of laser-induced breakdown spectroscopy for analysis of geological materials. *Appl. Spectrosc. Rev.* **2015**, *50* (1), 1−26.
(68) Nagata, K.; Sugita, S.; Okada, M. Bayesian spectral deconvolution with the exchange Monte Carlo method. *Neural Networks* **2012**, *28*, 82−89.
(69) Cowan, R. D.; Dieke, G. H. Self-absorption of spectrum lines. *Rev. Mod. Phys.* **1948**, *20*, 418−455.

https://doi.org/10.1021/acsearthspacechem.4c00067
ACS Earth Space Chem. XXXX, XXX, XXX−XXX